Electronic Supplementary Material (ESI) for Nanoscale.

New stable isomophorous Ag_{34} and $Ag_{33}Au$ nanoclusters with an open shell electronic structure

Supplementary Information

Xiao-Juan Xi,[a] Jin-Sen Yang,[a] Jia-Yin Wang,[a] Xi-Yan Dong*[ab] and Shuang-Quan Zang*[a]

[a]*College of Chemistry and Molecular Engineering, Zhengzhou University, Zhengzhou 450001, China.*

[b]*College of Chemistry and Chemical Engineering, Henan Polytechnic University, Jiaozuo 454000, China.*

*E-mail: dongxiyan0720@hpu.edu.cn (X-Y Dong); zangsqzg@zzu.edu.cn (S-Q Zang)

Materials and Methods

Materials and reagents

All the chemicals and reagents used in our study were of commercially available reagent grade and were used as received without any additional purification, including silver nitrate ($AgNO_3$), trifluoroacetic acid, chloro(triphenylphosphine)gold(I) [$AuClPPh_3$], benzyl mercaptan ($HSCH_2Ph$), triphenylphosphine, 3-bdppmapy was synthesized as reported before.[1] Solvents and other chemicals including methanol, ethanol, N,N-Dimethylformamide (DMF), and dichloromethane (DCM).

Characterization

The thermogravimetric (TG) analyses of the as-synthesized nanoclusters were performed on a SDT 2960 thermal analyzer from room temperature to 400 ℃ at a heating rate of 10 ℃/min under nitrogen atmosphere. UV-vis absorption spectra was recorded with a U-2000 spectrophotometer, and solution samples were prepared using CH_2Cl_2 as the solvent. ICP-OES measurements were carried out using an Aglient 720 inductively coupled plasma optical emission spectrometer. TEM images were recorded using an electron microscope (Hitachi, JEM-2100F). ESI-Mass spectra were obtained using an Agilent 6420 Triple Quad LC/MS spectrometer. X-ray photoelectron spectroscopy (XPS) measurements were carried out using a VG Scientific ESCALAB 250 system with an Al Kα (300 W) X-ray resource. FTIR spectra were analysed on a Nexus 870 FTIR spectrometer from KBr pellets as the sample matrix. EDS measurement was collected using Zeiss Sigma 500. Electrochemical measurements were conducted with an electrochemical analyser (CHI 660E), a glassy carbon working electrode, a SCE reference electrode, and a Pt wire counter electrode in 0.1 M $^nBu_4NPF_6/CH_2Cl_2$. Prior to use, the working electrode was polished using 0.05μm alumina powder, followed by sonication in redistilled water and ethanol respectively. The electrolyte solution was degassed with ultrahighpurity nitrogen for at least 40 min to remove the oxygen and blanketed with a nitrogen atmosphere during the entire test procedure.

Powder X-ray diffraction (PXRD)

Powder X-ray diffraction (PXRD) data were performed at room temperature in air using X'Pert PRO diffractometer (Cu Kα, λ = 1.54178 Å).

Single-crystal X-ray diffraction Analysis (SCXRD)

SCXRD measurements were performed on a Rigaku XtaLAB Pro diffractometer with Cu-Kα radiation (λ = 1.54178 Å) at 150 K. Data collection and reduction were performed using the program CrysAlisPro.[2] The intensities were corrected for absorption using the empirical method implemented in SCALE3 ABSPACK scaling algorithm. The structures were solved with intrinsic phasing methods (*SHELXT-2015*)[3], and refined by full-matrix least squares on F^2 using *OLEX2*, which utilizes the *SHELXL-2015* module.[4] Imposed restraints in least-square refinement of each structure were commented in the corresponding CIF files. Thus only a general description of the structural refinement strategy is presented here. All

non-hydrogen atoms were refined anisotropically, and the hydrogen atoms were included on idealized positions. In addition, modeling of electron density within the voids of the frameworks did not lead to identification of guest (DMF) entities in structures, which is due to the seriously disorder arising from the quite weak interaction between guest and the host framework as well as the high lattice symmetry. Thus, the remaining electron density was flattened out using the solvent masking protocol inside *OLEX2* which results in a decrease in the final R value.

Preparation of $[Ag_{34}S_2(PhCH_2S)_{18}(CF_3COO)_9(C_3H_7NO)_6]$

$AgPhCH_2S$ (0.2 g, 0.9 mmol), CF_3COOAg (0.3 g, 1.4 mmol) and 3-bdppmapy (0.2 g, 0.4 mmol) were dissolved in a mixed solvent of CH_2Cl_2, and DMF (1:1) with the addition of 10 μL NEt_3 under stirring. The red solution was slowly evaporated in room temperature. After twenty days 29.5 mg black hexagons was obtained (8.3% based on $AgPhCH_2S$).

Preparation of $[Ag_{33}AuS_2(PhCH_2S)_{18}(CF_3COO)_9(C_3H_7NO)_6]$.

The cluster of $[Ag_{33}AuS_2(PhCH_2S)_{18}(CF_3COO)_9(C_3H_7NO)_6]$ was prepared in a similar procedure for $[Ag_{34}S_2(PhCH_2S)_{18}(CF_3COO)_9(C_3H_7NO)_6]$ with addition $AuPPh_3Cl$ (0.016 g, 0.03mmol). After one month, 36.8 mg black hexagons was obtained (10.2% based on $AgPhCH_2S$).

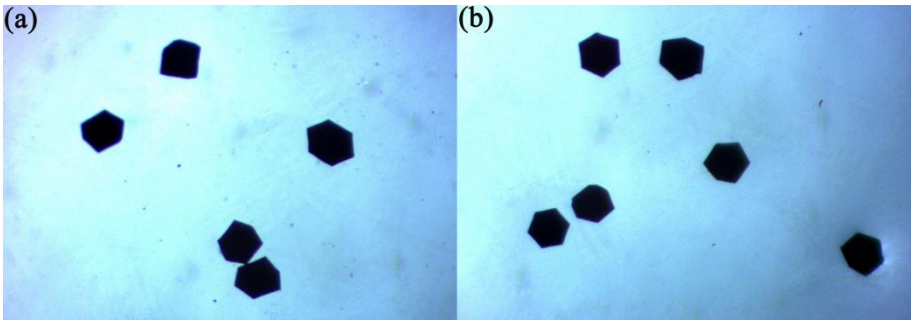

Figure S1. Photographs for crystals of (a) **Ag_{34}**, (b) **$Ag_{33}Au$**.

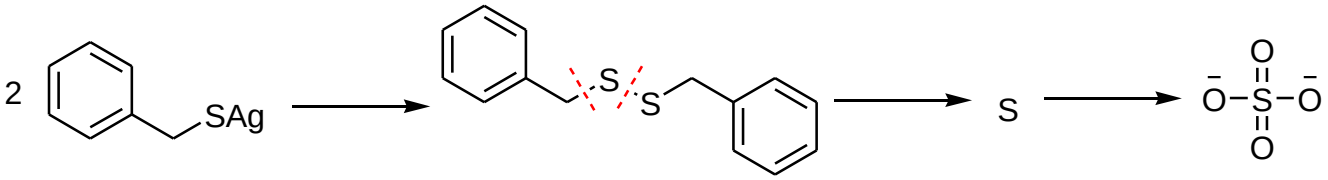

Figure S2. A proposed mechanism of the oxidation of thiol ligand during the reaction. The mechanism of the first step in the transformation is reasonable similar to in previous reported Au nanocluster work;[5] the reaction from disulfide to sulfate ion is available in the weakly oxidative conditions.[6] We also got the by-product sulfate ion compound in our proposed mechanism in a similar reaction and characterized its structure by single x-ray diffraction (Figure S3). The more detailed mechanism will be investigated in our future work.

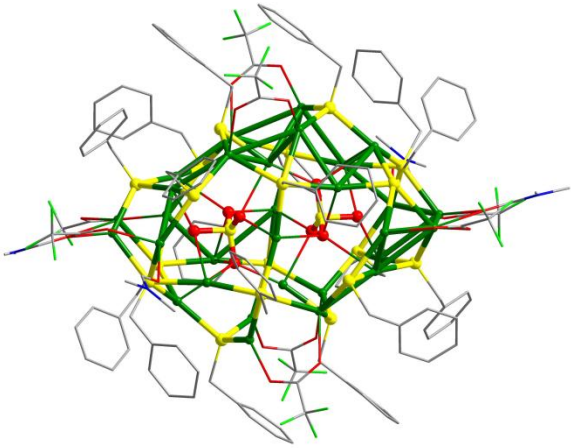

Figure S3. Crystal structure of the by-product sulfate ion compound $Ag_{30}(PhCH_2S)_{18}(SO_4)_2(CF_3COO)_8(DMF)_4$ (**Ag_{30}**) during the reaction.

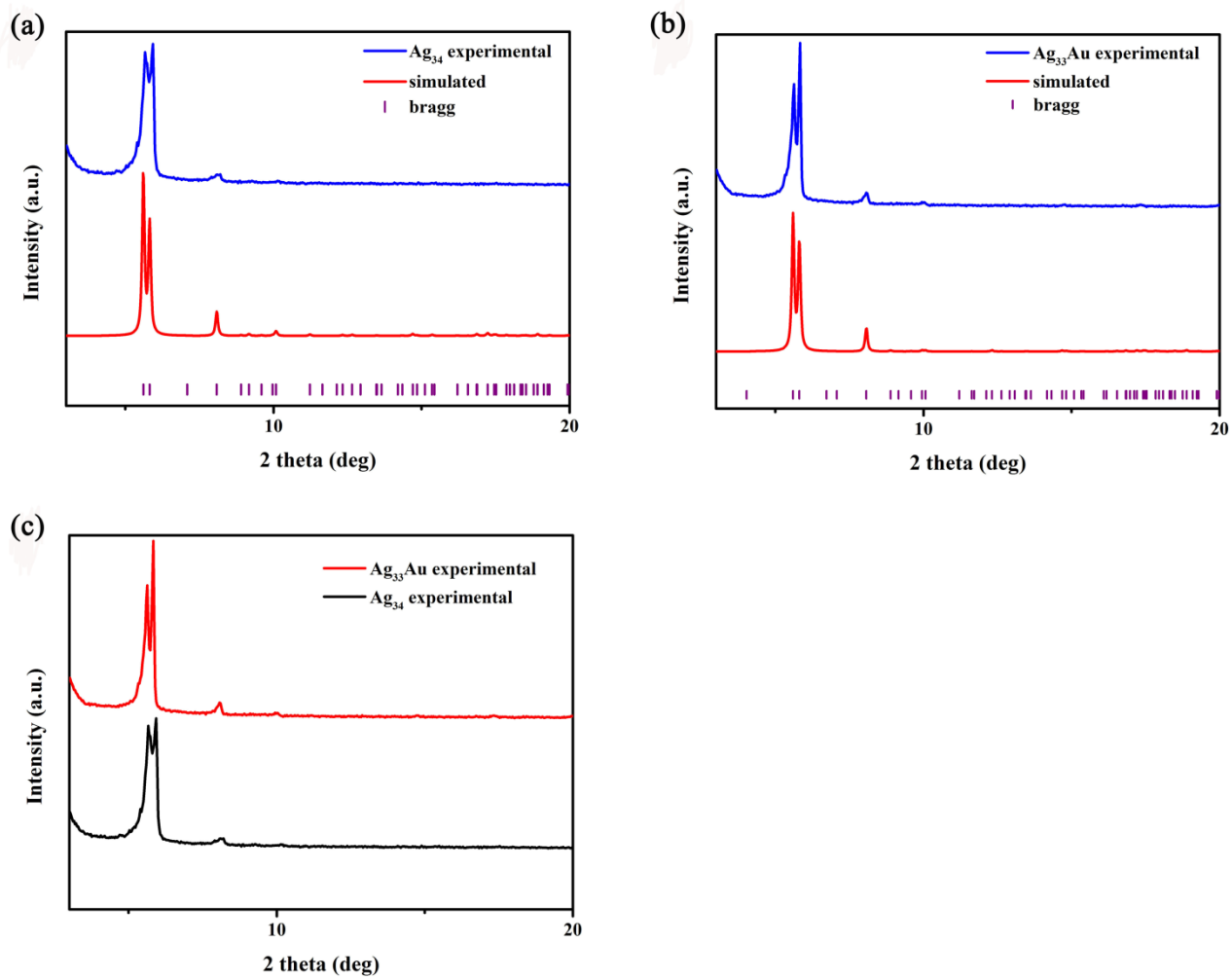

Figure S4. (a) PXRD analysis of **Ag_{34}**; (b) PXRD analysis of **$Ag_{33}Au$**; (c) PXRD analysis of **Ag_{34}** and **$Ag_{33}Au$**.

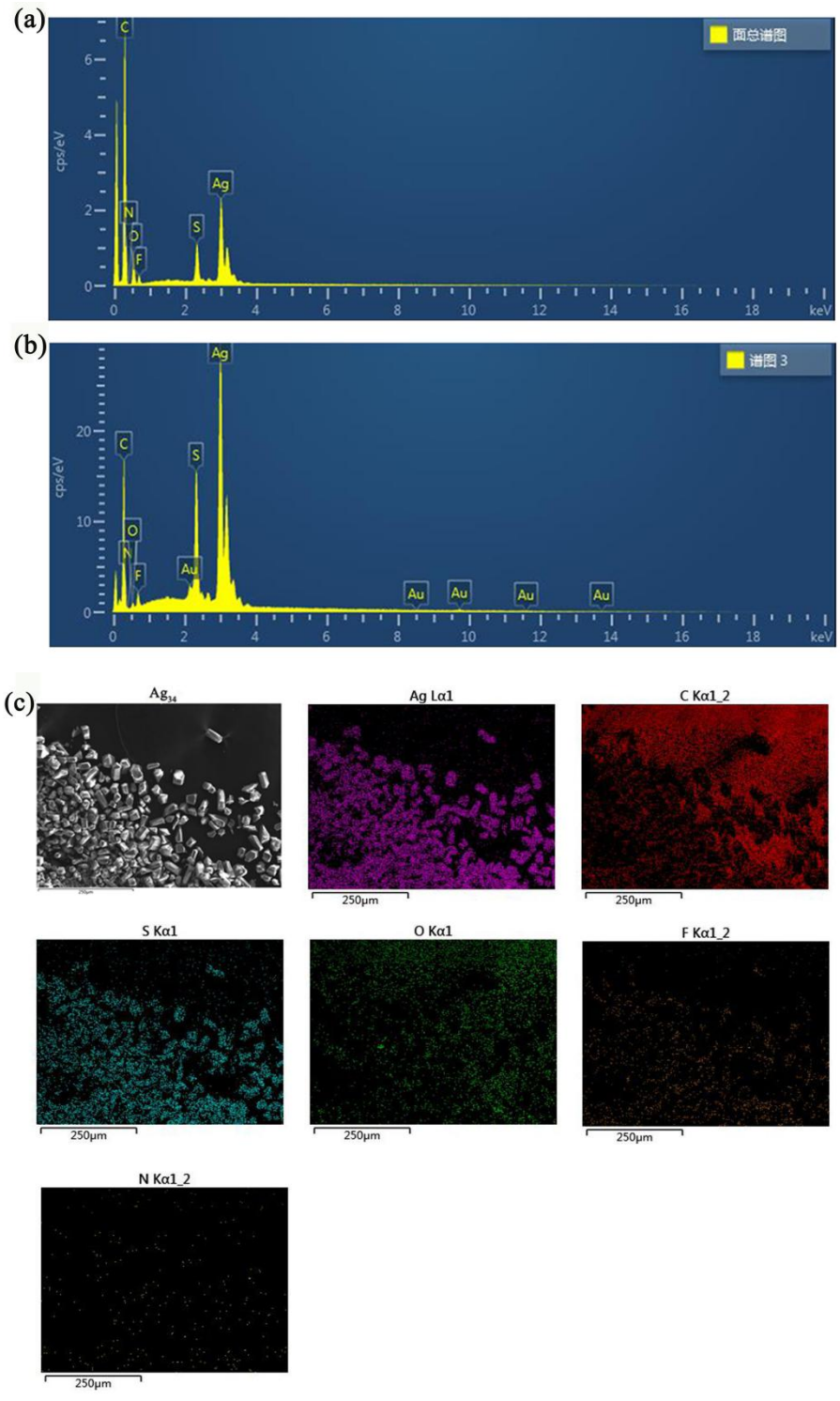
(a)
面总谱图
C
N
O
F
S
Ag
cps/eV
keV
(b)
谱图 3
C
O
N
F
S
Au
Ag
cps/eV
keV
(c)
Ag34
Ag Lα1
C Kα1_2
S Kα1
O Kα1
F Kα1_2
N Kα1_2
250μm

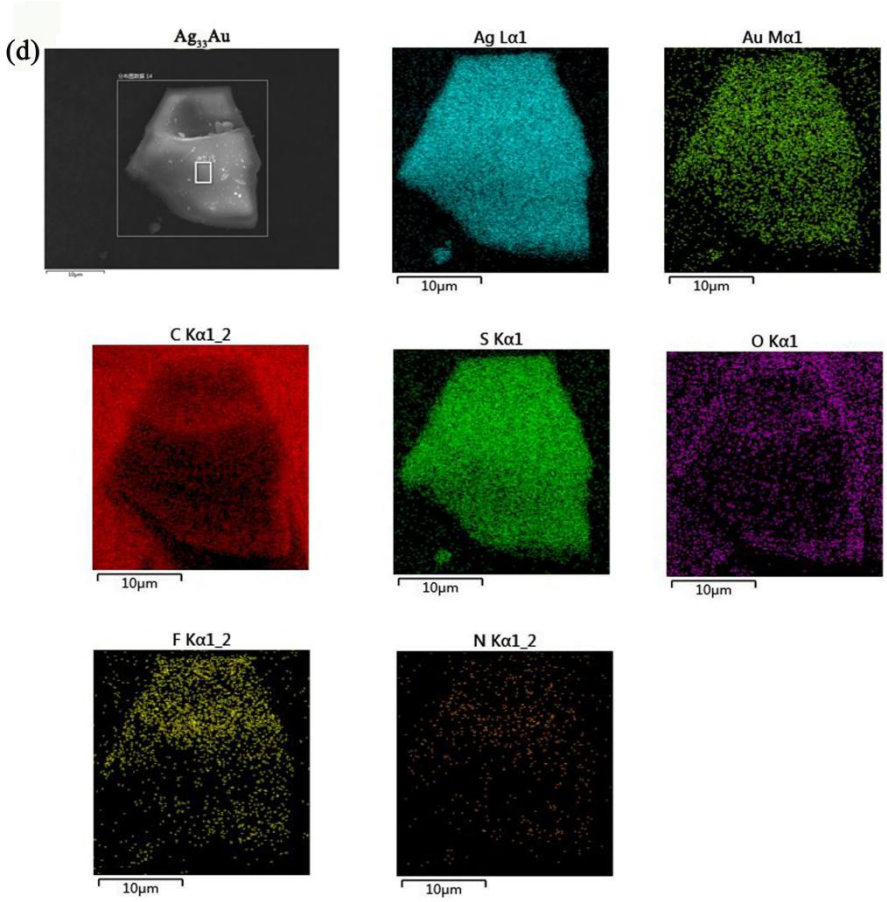

Figure S5. Energy Dispersive Spectrometer (EDS) analysis of **Ag_{34}** (a) and **$Ag_{33}Au$** (b); Elemental mapping images of **Ag_{34}** (c) and **$Ag_{33}Au$** (d).

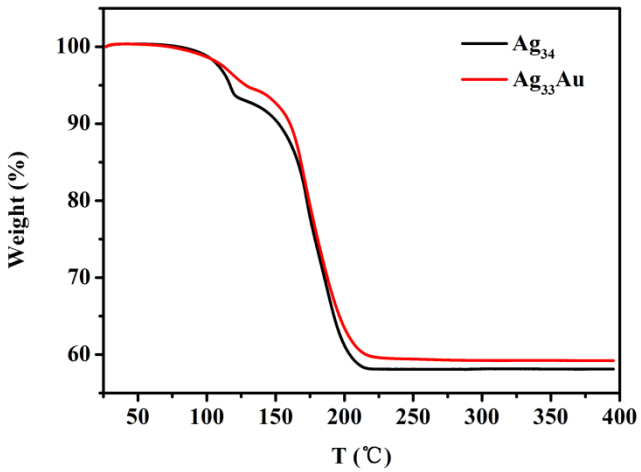

Figure S6. Thermogravimetric analysis of as-synthesized **Ag_{34}**, **$Ag_{33}Au$** under N_2 atmosphere.

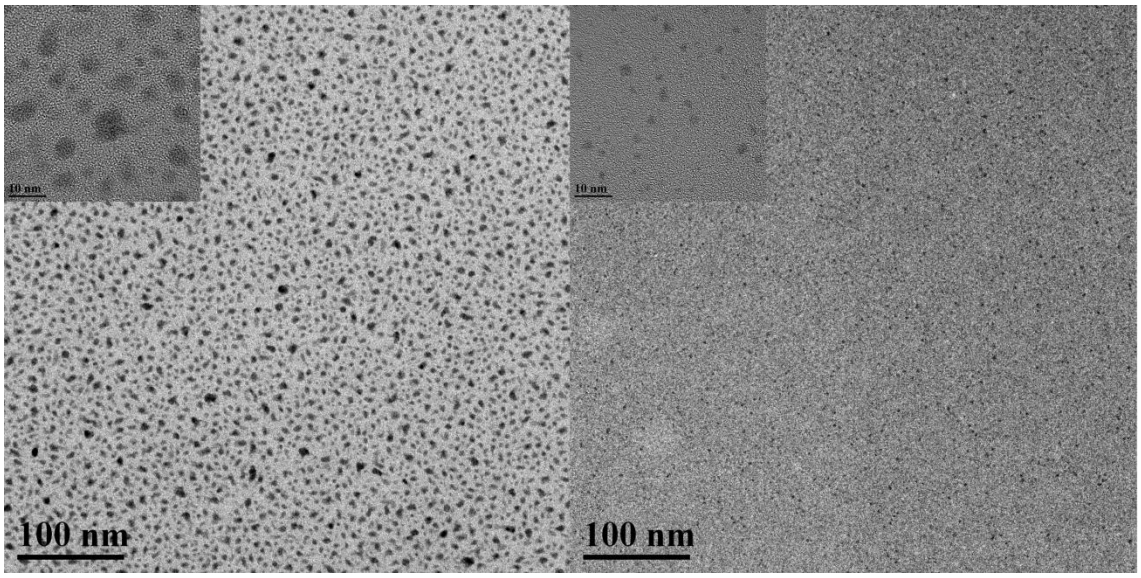

Figure S7. (a) TEM images of the as-prepared **Ag_{34}** nanoclusters; (b) TEM images of the as-prepared **$Ag_{33}Au$** nanoclusters. The inset is a representative high-magnification TEM image of the nanoclusters.

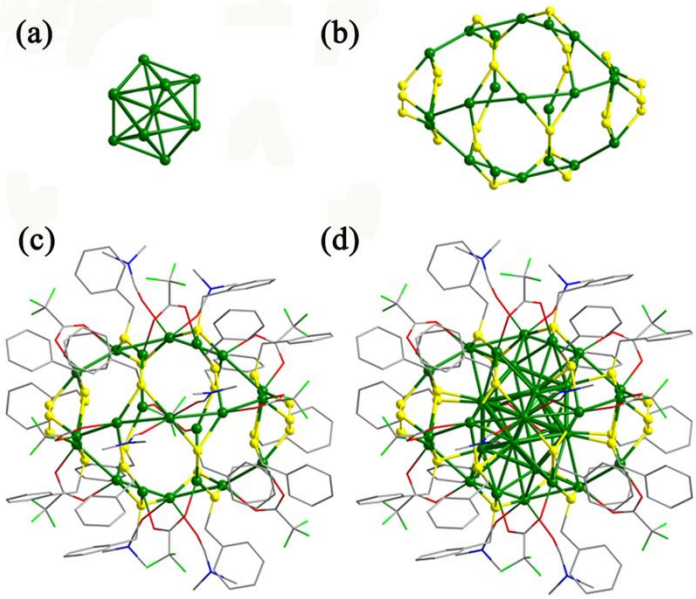

Figure S8. Anatomy of the structure of **Ag_{34}** showing the core-shell configuration and the position of the Ag atoms: (a) Ag_{13} centered icosahedral core; (b) simplified shell with omit the CF_3COO^- and DMF ligands; (c) shell structure; (d) X-ray structure of **Ag_{34}**. Color lables: Ag, green; S, yellow; N, blue; O, red; all H atoms are omitted for clarity.

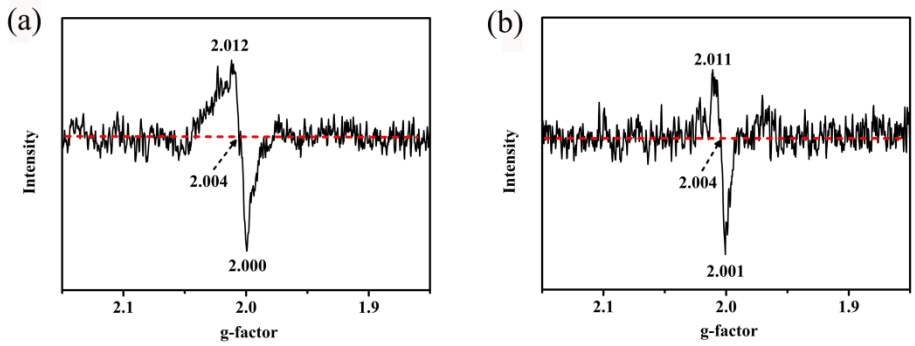

Figure S9. EPR spectrum of the (a) **Ag_{34}**; (b) **$Ag_{33}Au$** nanoclusters.

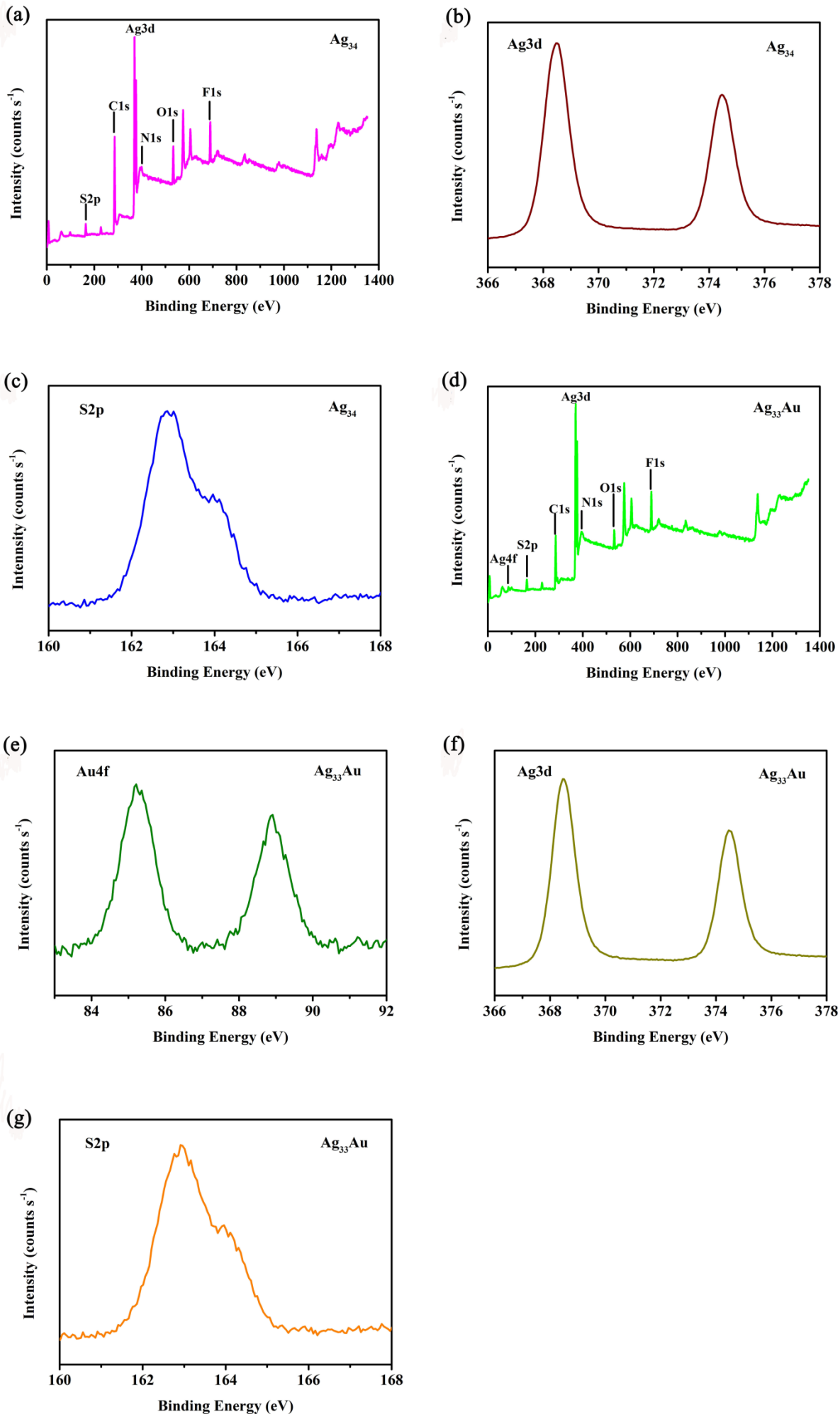
(a)
Ag3d
Ag34
C1s
O1s
F1s
N1s
S2p
Intensity (counts s-1)
0 200 400 600 800 1000 1200 1400
Binding Energy (eV)
(b)
Ag3d
Ag34
Intensity (counts s-1)
366 368 370 372 374 376 378
Binding Energy (eV)
(c)
S2p
Ag34
Intennsity (counts s-1)
160 162 164 166 168
Binding Energy (eV)
(d)
Ag3d
Ag33Au
F1s
O1s
C1s
N1s
S2p
Ag4f
Intensity (counts s-1)
0 200 400 600 800 1000 1200 1400
Binding Energy (eV)
(e)
Au4f
Ag33Au
Intensity (counts s-1)
84 86 88 90 92
Binding Energy (eV)
(f)
Ag3d
Ag33Au
Intensity (counts s-1)
366 368 370 372 374 376 378
Binding Energy (eV)
(g)
S2p
Ag33Au
Intensity (counts s-1)
160 162 164 166 168
Binding Energy (eV)

Figure S10. (a) XPS survey scan of **Ag_{34}**; (b) Ag 3d XPS spectra of **Ag_{34}**; (c) S 2p XPS spectra of **Ag_{34}**; (d) XPS survey scan of **$Ag_{33}Au$**; (e) Au 4f XPS spectra of **$Ag_{33}Au$**; (f) Ag 3d XPS spectra of **$Ag_{33}Au$**; (g) S 2p XPS spectra of **$Ag_{33}Au$**.

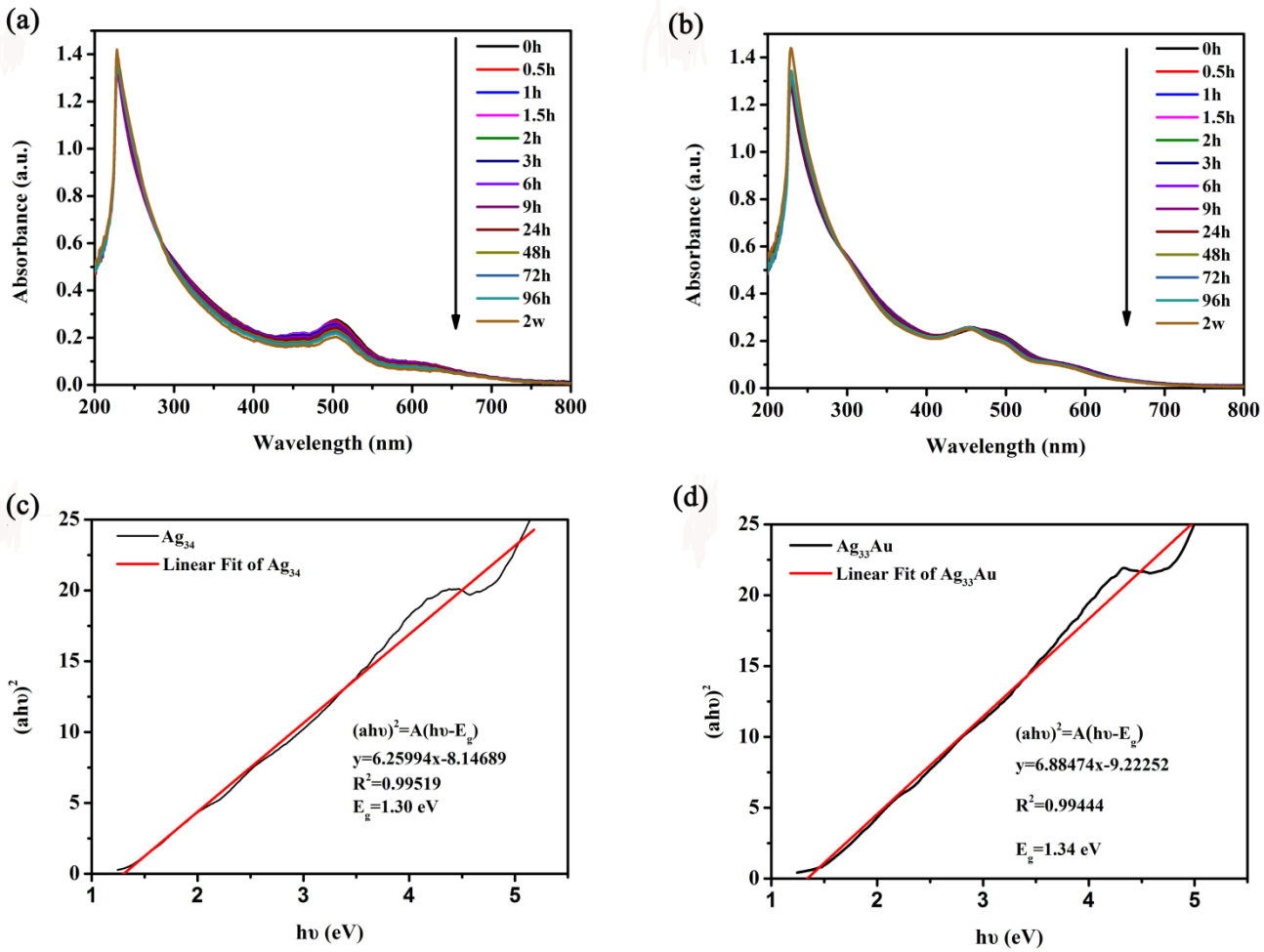

Figure S11. (a) Time-dependent UV-vis spectrum of **Ag_{34}** in CH_2Cl_2 solution; (b) Time-dependent UV-vis spectrum of **Ag_{34}** in CH_2Cl_2 solution; (c) Tauc plot displaying the band gap of **Ag_{34}**; (d) Tauc plot displaying the band gap of **$Ag_{33}Au$**.

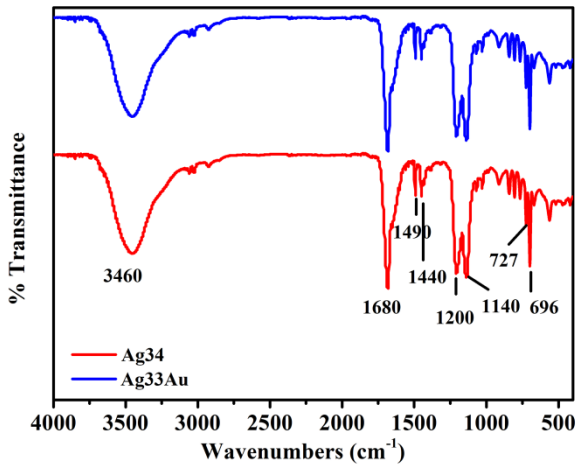

Figure S12. The IR spectra of **Ag_{34}**, **$Ag_{33}Au$**.

Table S1. Comparison of bond lengths in **Ag_{34}** and **$Ag_{33}Au$** clusters.

Ag_{34}	$Ag_{33}Au$

Center–$Ag_{icosahedron}$	2.7960 -2.8072 Å (average: 2.8021 Å)	2.7952-2.8064 Å (average: 2.8008 Å)
$Ag_{icosahedron}$–$Ag_{icosahedron}$	2.8743-3.0972 Å (everage: 2.9467 Å)	2.8925-3.0780 Å (everage: 2.9452 Å)
$Ag_{icosahedron}$–S	2.508 -2.578 Å (average: 2.543 Å)	2.495-2.570 Å (average: 2.533 Å)
Ag_{shell}–S	2.312-2.555 Å (average: 2.455 Å)	2.322-2.554 Å (average: 2.451 Å)

Table S2. Crystallographic data and structure refinement for **Ag_{34}** and **$Ag_{33}Au$**.

	Ag_{34}	$Ag_{33}Au$	Ag_{30}
CCDC number	1868083	1868082	1868081
Empirical formula	$C_{162}H_{168}Ag_{34}F_{27}N_6O_{24}S_{20}$	$C_{162}H_{168}Ag_{33}AuF_{27}N_6O_{24}S_{20}$	$C_{154}H_{154}Ag_{30}F_{24}N_4O_{28}S_{20}$
Formula weight	7404.79	7493.89	6842.10
Temperature / K	150.00(10)	150.01(10)	200.00(10)
Crystal system	trigonal	trigonal	monoclinic
Space group	R-3c	R-3c	$P2_1/n$
a / Å	30.3700(4)	30.3706(5)	19.8067(2)
			21.3657(2)
c / Å	39.4849(6)	39.4126(8)	24.6098(3)
α /°	90	90	90
			94.9090(10)
γ /°	120	120	90
Volume /$Å^3$	31539.2(10)	31482.8(12)	10376.27(19)
Z	6	6	2
ρ_{cale} g/cm^3	2.339	2.372	2.190
μ /mm^{-1}	27.293	27.889	24.681
F(000)	21210.0	21402.0	6552.0
Crystal size/mm^3	0.16 × 0.15 × 0.14	0.16 × 0.15 × 0.14	0.16 × 0.15 × 0.14
Radiation	Cu K*α* (λ=1.54184)	Cu K*α*(λ=1.54184)	Cu K*α*(λ=1.54184)
2θ range for data collection /°	5.598 to 146.522	5.604 to 146.582	5.486 to 148.584
Index ranges	-18 ≤ *h* ≤ 29	-34 ≤ *h* ≤ 37	-21 ≤ *h* ≤ 24
	-37 ≤ *k* ≤ 23	-35 ≤ *k* ≤ 36	-14 ≤ *k* ≤ 25
	-49 ≤ *l* ≤ 48	-34 ≤ *l* ≤ 48	-30 ≤ *l* ≤ 15
Reflections collected	26916	31150	48870
Independent reflections	6929 [R_{int}=0.0363, R_{sigma}=0.0308]	6945 [R_{int}=0.0439, R_{sigma}=0.0370]	20293 [R_{int}=0.0575, R_{sigma}=0.0717]
Data/restraints/parameters	6929/281/469	6945/312/519	20293/1716/1228
Goodness-of-fit on F^2	1.033	1.022	1.077
Final *R* indexes [I>=2σ(I)]	R_1=0.0600, wR_2=0.1731	R_1=0.0536, wR_2=0.1472	R_1=0.0584, wR_2=0.1537
Final R indexes [all data]	R_1=0.0797, wR_2=0.1941	R_1=0.0796, wR_2=0.1718	R_1=0.0790, wR_2=0.1617
Largest diff. peak/hole / e $Å^{-3}$	1.99/-1.17	2.07/-1.33	1.90/-2.61

$R_1 = \sum||F_o|-|F_c||/\sum|F_o|$. $wR_2 = [\sum w(F_o^2 - F_c^2)^2/\sum w(F_o^2)^2]^{1/2}$

Table S3. Ag-Ag, Ag-S and Ag-O bond length in **Ag_{34}**.

Ag1-Ag2#1	2.7961(6)	Ag3-Ag5#5	3.0311(12)
Ag1-Ag2#2	2.7960(6)	Ag3-Ag6#5	3.0542(11)
Ag1-Ag2#3	2.7961(6)	Ag3-S1	2.578(3)
Ag1-Ag2#4	2.7962(6)	Ag4-Ag4#3	3.2014(15)
Ag1-Ag2#5	2.7962(6)	Ag4-S1	2.465(3)

Ag1-Ag3#5	2.8070(6)	Ag4-S2	2.463(3)
Ag1-Ag3	2.8071(6)	Ag4-O2	2.346(8)
Ag1-Ag3#1	2.8072(6)	Ag5-Ag6#1	3.0678(11)
Ag1-Ag3#3	2.8072(6)	Ag5-Ag6	3.0676(11)
Ag1-Ag3#2	2.8072(6)	Ag5-S2#1	2.440(3)
Ag1-Ag3#4	2.8072(6)	Ag5-S2	2.440(3)
Ag2-Ag2#5	2.9089(12)	Ag5-O1	2.507(11)
Ag2-Ag2#4	2.9090(11)	Ag5-O1#1	2.507(11)
Ag2-Ag3#1	3.0202(9)	Ag6-Ag7	2.9623(19)
Ag2-Ag3#5	2.9139(9)	Ag6-S1#4	2.555(3)
Ag2-Ag3#4	2.9031(9)	Ag6-S2	2.506(3)
Ag2-Ag4#4	2.9726(10)	Ag6-O3	2.317(9)
Ag2-Ag6#4	3.0098(11)	Ag7-S3#5	2.495(3)
Ag2-S3	2.508(3)	Ag7-S3	2.416(3)
Ag3-Ag3#3	3.0972(13)	Ag7-S4	2.312(10)
Ag3-Ag3#2	2.8743(13)	Ag7-O4	2.264(10)
Ag3-Ag4	2.9950(10)	Ag1-Ag2	2.7961(6)
Ag3-Ag4#3	3.0002(10)		

Symmetry codes: #1: 2/3-*y*+*x*, 4/3-*y*, 5/6-*z*; #2: 2/3-*x*, 1/3-*x*+*y*, 5/6-*z*; #3: -1/3+*y*, 1/3+*x*, 5/6-*z*; #4: +*y*-*x*, 1-*x*, +*z*; #5: 1-*y*, 1+*x*-*y*, +*z*

Table S4. Ag-Ag, Ag-Au, Ag-S and Ag-O bond length in **$Ag_{33}Au$**.

Ag1-Ag1#1	3.0780(14)	Ag3-O1	2.277(10)
Ag1-Ag1#2	2.8963(13)	Ag3-S3#4	2.503(3)
Ag1-Ag2#3	2.9200(10)	Ag3-S3	2.407(3)
Ag1-Ag2#4	2.8925(10)	Ag3-S4	2.322(10)
Ag1-Ag2#5	3.0257(9)	Ag4-Ag5	3.0601(11)
Ag1-Ag4#4	3.0576(11)	Ag4-O2	2.341(9)
Ag1-Ag5#4	3.0257(12)	Ag4-S1#3	2.554(3)
Ag1-Ag6#1	3.0016(10)	Ag4-S2	2.515(3)
Ag1-Ag6	2.9898(10)	Ag5-O3#5	2.544(12)
Ag1-Au1	2.8064(7)	Ag5-O3	2.544(12)
Ag1-S1	2.570(3)	Ag5-S2	2.441(3)
Ag2-Ag2#3	2.9021(12)	Ag5-S2#5	2.442(3)
Ag2-Ag2#4	2.9020(12)	Ag6-Ag6#1	3.1943(16)
Ag2-Ag4#3	3.0150(12)	Ag6-O4	2.352(8)
Ag2-Ag6#3	2.9883(10)	Ag6-S1	2.468(3)
Ag2-Au1	2.7952(6)	Ag6-S2	2.462(3)
Ag2-S3	2.495(3)	Ag3-Ag4	2.9554(19)

Symmetry codes: #1: 4/3-*X*,2/3-*X*+*Y*,7/6-*Z*; #2: 1/3+*Y*,-1/3+*X*,7/6-*Z*; #3: 1-*Y*,+*X*-*Y*,+*Z*; #4: 1+*Y*-*X*,1-*X*,+*Z*; #5: 1/3-*Y*+*X*,2/3-*Y*,7/6-*Z*

Reference

[1] J. F. Wang, S. Y. Liu, C. Y. Liu, Z. G. Ren and J. P. Lang, Dalton Trans., 2016, **45**, 9294-9306.

[2] CryaAlisPro 2012, Aligent Technologies. Version 1.171.36.31.

[3] G. M. Sheldrick, Acta Crystallogr. Sect. A 2015, **71**, 3-8.

[4] O. V. Dolomanov, L. J. Bourhis, R. J. Gildea, J. A. K. Howard, H. Puschmann, OLEX2: a complete structure solution, refinement and analysis program. J. Appl. Cryst. 2009, **42**, 339-341.

[5] Z. Y. Wang, M. Q. Wang, Y. l. Li, P. Luo, T. T. Jia, R. W. Huang, S. Q. Zang and T. C. W. Mak, J. Am. Chem. Soc., 2018, **140**, 1069-1076.

[6] S. B. Moosun, L. H. Blair, S. J. Coles, S. J. Laulloo and M. G. Bhowon, Z. Anorg. Allg. Chem., 2015, **641**, 890-895.